Time-Resolved Site-Directed Spin-Labeling Studies of Bacteriorhodopsin: Loop-Specific Conformational Changes in M†

Ramin Mollaaghababa,‡,§ Heinz-Jürgen Steinhoff,|| Wayne L. Hubbell,*,⊥ and H. Gobind Khorana*,‡

Departments of Biology and Chemistry, Massachusetts Institute of Technology, Cambridge, Massachusetts 02139, Institut für Biophysik, Ruhr-Universität Bochum, 44780 Bochum, Germany, and Jules Stein Eye Institute and Department of Chemistry and Biochemistry, University of California, Los Angeles, California 90095-7008

Received August 20, 1999; Revised Manuscript Received November 12, 1999

ABSTRACT: A spin-label at site 101 in the C−D loop of bacteriorhodopsin was previously found to detect a conformational change during the M → N transition [Steinhoff, H. -J., Mollaaghababa, R., Altenbach, C., Hideg, K., Krebs, M. P., Khorana, H. G., and Hubbell, W. L. (1994) *Science 266*, 105−107]. We have extended these time-resolved electron paramagnetic resonance studies in purple membranes by analyzing conformational changes detected by a spin-label at another site in the C−D loop (103), and at sites in the A−B loop (35), the D−E loop (130), and the E−F loop (160). In addition, we have investigated the motion detected by a spin-label at site 101 in a D96A mutant background that has a prolonged M intermediate. We find that among the examined sites, only spin-labels in the C−D loop detect a significant change in the local environment after the rise of M. Although the D96A mutation dramatically prolongs the lifetime of the M intermediate, it does not perturb either the structure of bacteriorhodopsin or the nature of the light-activated conformational change detected by a spin-label at site 101. In this mutant, a conformational change is detected during the lifetime of M, when no change in the 410 nm absorbance is observed. These results provide direct structural evidence for the heterogeneity of the M population in real time, and demonstrate that the motion detected at site 101 occurs in M, prior to Schiff base reprotonation.

Bacteriorhodopsin (BR)[1] is a light-driven proton pump residing in the plasma membrane of the archeon *Halabacterium halobium (*also referred to as *H. salinarium*) in the form of two-dimensional crystalline sheets known as the purple membrane (*1*). BR contains seven transmembrane regions and one bound molecule of *all-trans*-retinal, covalently attached via a Schiff base moiety at the ϵ-amino group of lysine 216 (*2*) (Figure 1). BR undergoes a cyclic series of transformations upon light absorption by its retinal chromophore, resulting in the conversion of the harvested light energy into chemical energy by net transport of protons from the cytoplasmic space to the extracellular milieu (*3*). The BR photocycle can be conceptually described as being composed of two halves (Figure 2). In the first half of the cycle, deprotonation of the Schiff base takes place during the transition of the L intermediate to the M intermediate. In the second half, the Schiff base reprotonates during the M to N transition, and the cycle is subsequently completed. The mechanism of proton translocation during the photocycle has been the subject of intense biochemical and biophysical research over the past 2 decades (for selected reviews, see refs *3*−*7*). The identification of several key residues involved in the proton translocation pathway was made possible by site-directed mutagenesis studies of BR (*4*). In particular, these studies have shown that residue Asp 85 is the acceptor of the Schiff base proton during the first half of the photocycle (*8*−*11*). Moreover, the deprotonation of Asp 96 is required for the reprotonation of the Schiff base during the M to N transition in the second half (*8*, *12*−*16*).

Although the molecular mechanism of proton translocation by BR has been studied in detail in the past, a picture of the structural transitions that accompany its photocycle activity is just emerging. The existence of tertiary structural changes relative to BR under conditions where the M photointermediate accumulates has been independently established by time-resolved X-ray (*17*−*19*), electron microscopy (*20*, *21*), and neutron diffraction studies (*22*). Electron diffraction analysis of a mutant that accumulates the O intermediate has also revealed significant structural differences between this late intermediate and the unphotolyzed state (*23*). Additionally, secondary structural changes during the BR photocycle have been identified by time-resolved FTIR spectroscopy (for a review, see ref *16*).

SDSL has also been applied to detect protein movement during the photocycle. In the SDSL method, specific attach-

† This work was supported by NIH Grants GM28289 (to H.G.K.) and EY052.16 (to W.L.H.), the Jules Stein Professor Endowment (to W.L.H.), and the Max Kade Foundation Fellowship (to H.-J.S.).

* To whom correspondence should be addressed.

‡ Massachusetts Institute of Technology.

§ Current address: Genetic Disease Research, National Human Genome Research Institute, National Institutes of Health, Bethesda, MD 20892-4472.

|| Ruhr-Universität Bochum.

⊥ University of California, Los Angeles.

[1] Abbreviations: BR, bacteriorhodoopsin; EPR, electron paramagnetic resonance; SDSL, site-directed spin-labeling; MTSSL, methanethiosulfonate spin-label; FTIR, Fourier transform infrared.

10.1021/bi991963h CCC: $19.00
Published on Web 01/08/2000

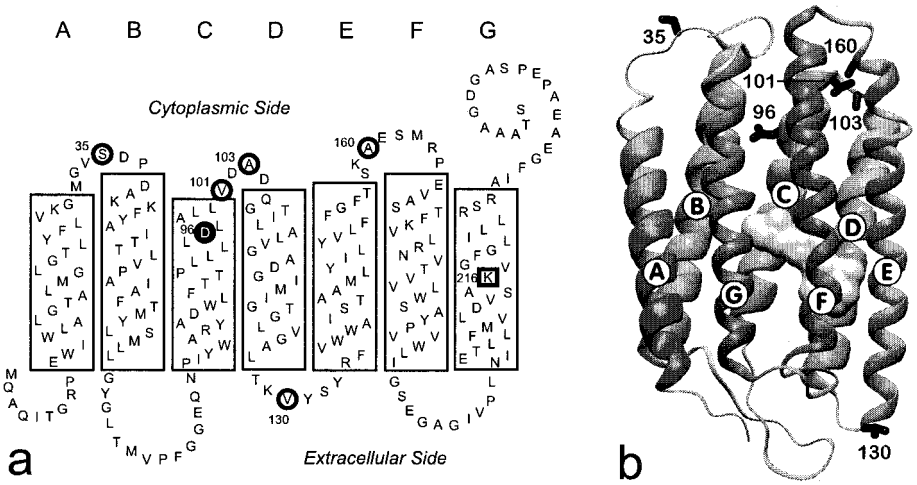

FIGURE 1: Structural model of bacteriorhodopsin. (a) Secondary structural model of bacteriorhodopsin. Boxed areas indicate helical segments according to the model of Grigorieff et al. (*54*). A box is also drawn around lysine 216, the attachment site for the *all-trans*-retinal chromophore. The circled amino acid residues within the loop regions were individually changed to cysteine. Residue D96, which was substituted with alanine in the double mutant D96A/V101C, is also designated. (b) BR backbone is shown in ribbon representation. The locations and orientations of the amino acid side chains that were modified in this study are highlighted. The coordinates were obtained from ref *55*.

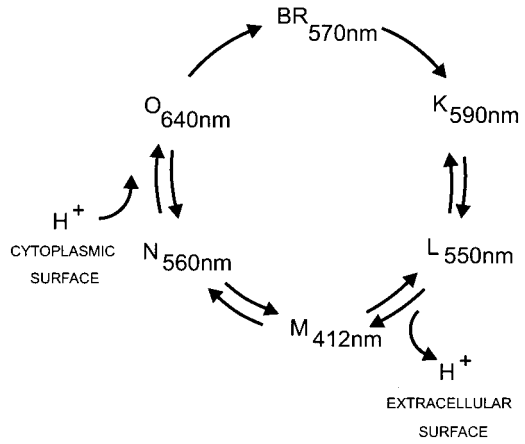

FIGURE 2: A current model of the BR photocycle. The wavelength of maximal absorbance for each intermediate is shown. As discussed in the text, the M intermediate consists of at least two structurally distinct species.

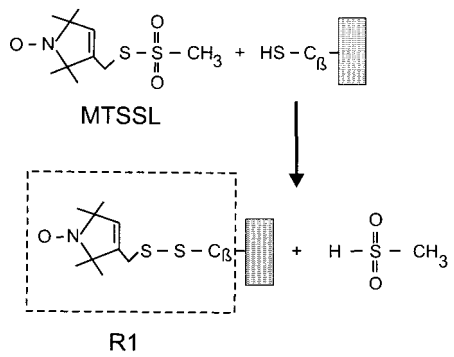

FIGURE 3: Chemical reaction of cysteine residues with (1-oxyl-2,2,5,5-tetramethylpyrroline-3-methyl)methanethiosulfonate (MTSSL) spin-label to generate the nitroxide side chain designated R1.

ment sites for spin-labels in a protein are provided by cysteine substitution mutagenesis. The sulfhydryl group of the unique cysteine is modified with a specific reagent to introduce a nitroxide side chain. The most commonly used reagent is the methanethiosulfonate spin-label, MTSSL, that generates the side chain designated R1 (Figure 3). The internal motion of R1 relative to the protein is reflected by the shape of the EPR spectrum, and this in turn provides information on the degree of interaction of the side chain with nearby groups in the protein (*24*). Consequently, a conformational change that perturbs the environment of the spin-label will result in changing the shape of the EPR spectrum. Such spectral changes can be detected on the millisecond time scale with time-resolved EPR spectroscopy (*25*). The first time-resolved EPR study of BR using SDSL showed the existence of conformational changes localized near the C−D or E−F interhelical loops during the second half of the photocycle (*26*, *27*). Subsequent SDSL analyses revealed smaller but detectable protein movements near both the A−B and E−F loops (*28*), and relative movement between the cytoplasmic loops was suggested by use of double-label SDSL (*29*).

The time-resolved EPR technique greatly complements the aforementioned diffraction methods for structural analysis of BR by providing several important and distinct advantages. Most significantly, it allows the detection of localized structural transitions in real time, using aqueous suspensions of purple membrane. This feature allows an unambiguous correlation of the observed conformational changes with photocycle kinetics. As a result, there is no need to work under nonphysiological experimental conditions in order to prolong the lifetime of specific intermediates. Additionally, because the technique relies on the sensitivity of an attached spin-label to its immediate environment, SDSL provides information on localized structural transitions. This is in contrast to the diffraction techniques used in BR analysis, which give information along the length of the molecule but do not provide localized spatial resolution.

In previous work referred to above (*26*), we used the SDSL technique to reveal a structural rearrangement near site 101 near the top of helix C (Figure 1) that occurred after M formation. Interestingly, a spin-label at site 105 in the same loop showed no changes with light excitation, and the implications of this difference have been discussed (*26*). In the present report, we extend our time-resolved EPR studies to probe for light-induced conformational changes at site 103, located between sites 101 and 105 in the C−D loop. In addition, we explore other loop regions of BR. The inter-

helical loops are targeted because previously published crystallographic work has not provided information on light-dependent movement in these regions. In addition, the cysteine mutations introduced in the loops were expected to be reasonably exposed to the aqueous medium and therefore amenable to modification by spin-labeling, as was the case with our previous attempts (*26*). We find that among the selected sites, only the spin-labels in the C−D loop detect significant photoinduced structural transition(s). The possibility that such significant changes may also be detected at additional specific sites in other loops cannot be ruled out at present, and requires further analysis of these regions. Nevertheless, our current results for the D−E interhelical loop, together with our previous observations for the B−C loop (*26*), are consistent with the finding that little light-dependent motion takes place in the extracellular side of BR (*20*).

Several reports have suggested the possibility that structurally distinct M species exist within the BR photocycle. These include results from spectroscopic measurements (e.g., *30*−*35*), electron diffraction (*36*), neutron diffraction (*37*), and a combination of FTIR and X-ray studies (*38*). In particular, it has recently been proposed that the protein conformation corresponding to the N intermediate takes shape prior to M decay, switching the Schiff base orientation so that it can become protonated during the M → N transition (*5*). The postulated pre-switch and post-switch states within M are referred to as M_1 and M_2, respectively (*32*). The FTIR analysis of the D96N mutant at pH 10 by Sasaki et al. (*35*) has shown the accumulation of what appears to be yet another distinct species, designated M_N. Despite having an N-like protein structure, the M_N intermediate has an unprotonated Schiff base. Time-resolved step−scan FTIR measurements provide evidence of its existence in D96N at neutral pH (*39*). However, no direct evidence is yet available for the existence of M_N in the wild-type photocycle under physiological conditions, where the reprotonation may occur too fast to allow the detection of this intermediate. Although previous diffraction studies have revealed changes in protein structure under conditions where M accumulates (*17*−*22*), they could not provide information on the timing of these changes with respect to M kinetics. More recently, Sass et al. (*38*) have suggested that the tertiary structural changes in M correspond to the $M_1 \rightarrow M_2$ transition based on parallel X-ray and FTIR studies of the D96N mutant at different relative humidity.

In the present paper, we take advantage of the time resolution that the SDSL technique provides to determine whether the motion that occurs at or near the C−D loop during the M → N transition (*26*) takes place in M. For this purpose, we investigated this major conformational change in a mutant background, which significantly slows the rate of M decay (D96A). The mutant D96A/V101R1 allowed a precise real-time comparison between the evolution of the major EPR spectral change and that for M. The experimental results presented here show that the conformational change takes place in M, at a time when the Schiff base is still unprotonated. Thus, our findings provide a real-time demonstration of the structural heterogeneity of M, and show that part of the conformational change in M involves movement at or near the C−D interhelical loop. These observations are consistent with and complement the available diffraction data on light-induced changes in BR.

EXPERIMENTAL PROCEDURES

Materials. The spin-label reagent (1-oxyl-2,2,5,5-tetramethylpyrroline-3-methyl)methanethiosulfonate (MTSSL, Figure 3) was obtained from Reanal (Budapest, Hungary). High-purity acetonitrile used in spin-labeling reactions was obtained from American Burdick and Jackson. Tempone (2,2,6,6-tetramethyl-4-oxopiperidine-1-oxyl) was from Aldrich. A. W. Alberts (Merck) was the generous provider of mevinolin, which was converted to the δ-hydroxy acid as described (*40*) and used in isolation of recombinants expressing BR mutants. The Genius DNA Labeling and Detection system of Boehringer Mannheim and the Enhanced Chemiluminescence Detection kit from Amersham were used for Southern blot analyses. The restriction enzymes and ligase were obtained from Boehringer Mannheim and New England Biolabs. A Qiagen plasmid kit was used for purification of the plasmids. Sequencing was by the Sequenase version 2.0 kit from U.S. Biochemical.

Plasmid Construction. The construct for the S35C mutation was obtained by combining the 6.7 kbp *Bam*HI−*Hin*dIII fragment of pMPK54 (*41*), the 476 bp *Bam*HI−*Nhe*I and 2.9 kbp Asp718−*Hin*dIII fragments of pMPK39 (*42*), and the 171 bp *Nhe*I−Asp718 synthetic fragment of pSBO2.S35C (*43*). Plasmids for D96A/V101C and A103C were prepared using the strategy previously described for the V101C mutation (*26*). The constructs for V130C and A160C were obtained by combining the 6.7 kbp *Bam*HI−*Hin*dIII fragment of pMPK54, the 2.48 kbp *Hin*dIII−*Psp*1406I and 781 bp *Bam*HI−*Bsp*HI fragments of pMPK39, and the 177 bp *Bsp*HI−*Psp*1406I synthetic fragments of pSBO2.V130C (*44*) and pSBO2.A160C (*43*), respectively. To verify the presence of the mutations, the entire synthetic fragment of each purified construct was sequenced.

Expression, Purification, and Characterization of Mutants in the Purple Membrane Form. The mutant proteins were expressed in the *bop* deletion strain MPK40 (*41*). Transformation of the MPK40 strain with each of the purified mutant constructs, isolation of recombinants and their characterization by Southern blot analysis, and purple membrane purification were performed as previously described (*41*). The MPK40 recombinant expressing WT(AB) (*41*) was used for preparation of purified wild-type purple membrane.

The purified samples were analyzed by SDS−PAGE on 12% polyacrylamide gels as described (*45*). UV/visible spectroscopy in both dark-adapted and light-adapted states was performed as previously described (*42*) using a Hitachi U-3110 spectrophotometer modified with an end-on photomultiplier. The photocycle kinetics for each sample were measured both before and after spin-labeling. For these measurements, photoexcitation was carried out using 100 μs light flashes at <550 nm wavelength. A probe beam was used with 410 and 570 nm interference filters in order to monitor the kinetics of the M intermediate and the unphotolyzed state, respectively.

Spin-Labeling of Cysteine Substitution Mutants and EPR Measurements. The single reactive cysteine residue in each of the BR mutants in purified purple membranes was modified by MTSSL (Figure 3; ref *26*). Wild-type BR purple membrane was included as control. The stock label solution was prepared using high-purity acetonitrile, and was stored at 4 °C under dim light. The labeling was performed in a

5-fold molar excess of the spin-label in 200 mM sodium phosphate buffer, pH 7.0, for 12 h at 25 °C, and under dim light conditions. Subsequently, six successive centrifugal washes of the membranes were performed with the labeling buffer to remove excess free label. The resulting spin-labeled mutants are designated by specifying the original residue, the sequence number, and the new residue. For example, S35R1 is a mutant in which the wild-type serine was replaced with R1.

For the EPR measurements, spin-labeled purple membrane was resuspended in 0.1 M sodium phosphate buffer, pH 7.0, containing 0.1 M NaCl. The concentration of each sample was calculated from its λ_{max} value in the light-adapted form, using the extinction coefficient $\epsilon = 63\,000\ M^{-1}\cdot cm^{-1}$ (*46*). For calculation of the labeling stoichiometry for each modified sample, double integration of the EPR spectra was performed and compared with that of a known amount of the water-soluble spin-label Tempone.

EPR spectra were recorded at X-band frequencies in a TM101 cavity at 25 °C. Light-induced changes of the EPR spectra were recorded during a magnetic field scan. This was accomplished by phase-sensitive detection, using as reference the triggering source of a xenon flash lamp with a 150 μs duration and 0.5 Hz repetition rate. Consequently, the difference EPR spectra between the photoexcited and unphotolyzed conformations were directly recorded. To correlate these light-induced changes with photocycle kinetics, the time dependence of the EPR signal after photoexcitation was measured with the magnetic field fixed at the maximum of the difference signal.

RESULTS

Characterization of the Cysteine Mutants: SDS−PAGE, UV/Visible Spectroscopy, and Photocycle Properties. SDS−PAGE analysis showed identical mobility for wild-type and mutant proteins. A single band was present for each sample, indicative of their high level of purity (*47*). The UV/visible spectra of all cysteine mutants used in this study were identical to the wild-type BR spectra in both dark- and light-adapted states (*47*). A $A_{280\ nm}/A_{568\ nm}$ absorbance ratio of 1.7−1.8 was obtained for the light-adapted species of the purified samples, confirming their high level of purity and indicating that they fold properly. The half-life of M decay for the wild-type purple membrane was found to be 3.9 ms. S35C and V130C mutants showed photocycle kinetics similar to those of the wild-type sample with the half-life values of 3.2 and 3.0 ms for M decay, respectively. The A103C mutation mildly perturbed the kinetics of M decay, slowing it by a factor of 1.3. This slight effect may actually be the consequence of a perturbation in the M−N equilibrium, emanating from a slower N decay. The rate of M decay was also retarded in the A160C mutant, which, like A103C, resides on the proton uptake side of the membrane. The photocycle kinetics of the A160C mutation have been described in detail (*48*). Consistent with the previous results, we found that the photocycle is slowed by a factor of 2 in A160C, with a half-life of 8 ms for M decay. As anticipated from previous observations for D96A (*12, 41*), the M decay was significantly delayed in the D96A/V101C mutation, occurring at a 500-fold slower rate (see below).

Properties of the Spin-Labeled Mutants in the Purple Membrane. For the single cysteine substitution mutants, the stoichiometry of MTSSL labeling was in the range of 0.7−0.9 mol of spin-label per mole of BR, consistent with the presence of a single cysteine residue. The wild-type BR, which is devoid of any cysteines, did not show detectable labeling with MTSSL, in agreement with previous results (*26*). The photoinduced properties of the labeled mutants were analyzed by measuring the optical density changes at 410 nm (M kinetics) and 570 nm (BR recovery). Spin-labeling of S35C, A103C, V130C, and A160C with MTSSL slowed M decay in these mutants by less than a factor of 2, with half-lives of 3.1, 3.8, 7.5, and 12 ms for S35R1, A103R1, V130R1, and A160R1, respectively. We previously found that spin-labeling of V101C with MTSSL slows the photocycle by a factor of 10 (*26*). In the D96A/V101R1 mutant, this effect is masked by the dramatic perturbation of M decay by the D96A mutation.

EPR Spectra of the Spin-Labeled Mutants in the Unphotolyzed State and Spectral Changes during the Photocycle. The mutants in this study were selected to investigate light-dependent conformational changes in the different loop regions of BR (Figure 1). Except for the V130C mutation, all sites are located on the cytoplasmic side of BR. The EPR spectra for the unphotolyzed states of the labeled mutants in purple membrane were obtained following full light-adaptation. The shapes of these spectra reflect the residual motion of the nitroxide side chain.

The light-induced EPR spectral changes for the mutants were measured during a magnetic field scan as described under Experimental Procedures. The detection scheme directly provides the difference EPR spectrum between the unphotolyzed state and the excited-state spectrum. Therefore, an interpretation of the difference spectrum provides information regarding the nature and relative magnitude of any light-induced conformational changes that modulate the spin-label environment. The EPR spectra in the unphotolyzed state and the spectral changes are discussed below for each mutant.

(A) S35R1 (A−B Interhelical Loop). The spectrum for this mutant is shown in Figure 4a, and reveals the presence of two dominant spin populations, reminiscent of R1 at tertiary contact sites (*49*). The high mobility of one population (arrow) suggests some contribution of backbone flexibility to the overall side-chain dynamics, as might be expected at an interhelical loop site. These findings are very similar to those reported for D36R1 (*28*).

Figure 4f shows the corresponding light-induced EPR difference spectrum for this mutation. Because the relative EPR spectral change is very small, the spectrum was amplified by a factor of 5 compared to the V101R1 and A103R1 spectra (to follow) in order to provide a better visualization of the signal. The shape of the EPR difference spectrum indicates a slight decrease in nitroxide mobility. However, given the high sensitivity of the spin-label to changes in its immediate environment (*24, 25*), we conclude that the light-induced conformational change at position 35 is likely to be small. These findings are similar to those for R1 at the adjacent site in D36R1 (*28*).

(B) D96A/V101R1 and A103R1 (C−D Interhelical Loop). The D96A/V101R1 spectrum is shown in Figure 4b. The spectral line shape corresponds to intermediate immobilization of the spin-label, and is virtually indistinguishable from that of V101R1 described previously (*26*) (dashed trace in Figure 4b). Therefore, in the unphotolyzed state, the substitu-

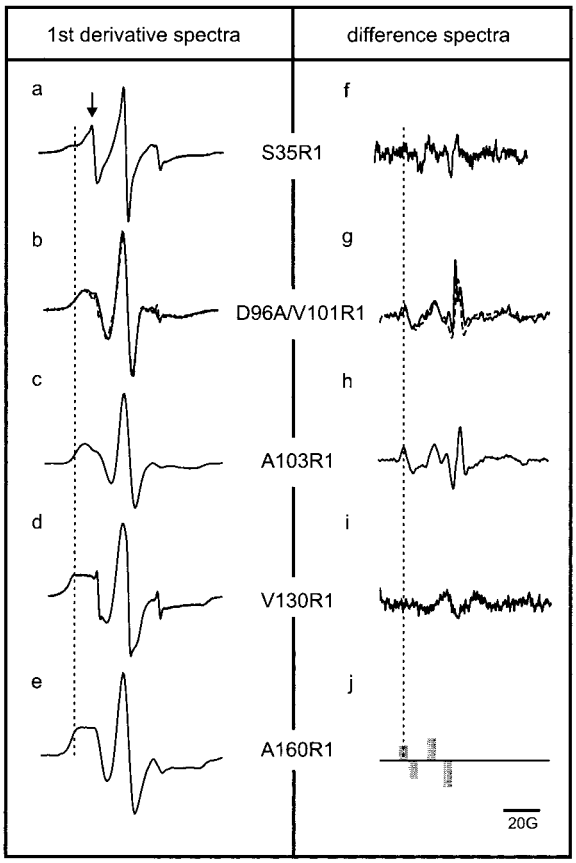

FIGURE 4: EPR spectra in the unphotolyzed state (a−e) and difference spectra obtained during the photocycle (f−j) for the indicated spin-labeled mutants. The arrow in (a) indicates the spin population with high mobility for S35R1. For comparison, the spectra for V101R1 (dashed lines in b and g) are superimposed with those of D96A/V101R1 (solid lines in b and g). The difference spectra for S35R1 (f) and V130R1 (i) are magnified by a factor of 5 with respect to those of V101R1 and D96A/V101R1 (g) in order to give a better visualization of the signal. Light-induced EPR changes for A160R1 were measured at discrete *B*-field values to the improve signal-to-noise ratio (j). The direction of change at these selected values is shown by the solid bars, and the length of each bar corresponds to the magnitude of the observed change. The positions of the outer hyperfine extrema that indicate nitroxide immobility are shown by dotted vertical lines.

tion D96A does not introduce any detectable structural changes in the vicinity of the spin-label probe at site 101.

The spectrum of A103R1 in the unphotolyzed state is shown in Figure 4c. The A103R1 spectrum reflects a nitroxide with distinctly less mobility than that at V101R1, suggesting that this region of the loop is highly ordered and likely in tertiary contact with other parts of the protein, consistent with the available structural data (Figure 1b).

The EPR difference spectrum for D96A/V101R1, superimposed with that for V101R1 (dashed line), is shown in Figure 4g. For both spectra, the changes in amplitude at the extremes clearly indicate a decrease in nitroxide mobility. The magnitude of the EPR difference spectrum suggests that a comparatively large conformational change occurs at the vicinity of this site during the photocycle (Figure 4g). The data of Figure 4g also demonstrate that the light-induced spectral changes for V101R1 and D96A/V101R1 are virtually superimposable, appearing at identical magnetic field values and with the same shapes and magnitudes.

Similar to V101R1 and D96A/V101R1, the difference spectrum for A103R1 shows a dramatic light-dependent conformational change, concomitant with a decrease in nitroxide mobility (Figure 4h). This suggests that the structural transitions detected at sites 101 and 103 may be the same, especially since the time dependencies of their EPR spectral changes are very similar (see below).

(C) V130R1 (D−E Interhelical Loop). The spectrum for V130R1 in the unphotolyzed state in the lattice indicates strong immobilization of the attached nitroxide, implying a strong tertiary interaction (Figure 4d). Similar to S35R1, the relative EPR spectral change is very small for this mutant (Figure 4i), and therefore the difference spectrum shown is amplified by a factor of 5 compared to the V101R1 and A103R1 spectra. The spectral shape indicates a slight increase in the mobility of the nitroxide side chain. However, the light-induced conformational changes detected at this site must correspond to a very limited change in the spin-label environment.

(D) A160R1 (E−F Interhelical Loop). Figure 4e shows the spectrum for this mutant in the unphotolyzed state. Similar to V130R1 spectrum, it indicates a strong immobilization of the nitroxide. Because the difference spectrum for this mutant was of very low amplitude, we measured the EPR transients at discrete values of the B-field in order to improve the signal-to-noise ratio (Figure 4j). The relative amplitude of the spectral changes at the selected magnetic field values is similar to that of S35R1, and indicates a very slight decrease in nitroxide mobility. Accordingly, the light-induced changes associated with A160R1 must be small, similar in magnitude to those at S35R1 and V130R1.

Correlation between the Kinetics of the EPR Spectral Changes and the Kinetics of the M Photointermediates. For each spin-labeled mutant, the time dependence of the light-induced EPR signal was recorded at a fixed magnetic field corresponding to the maximum in the difference signal. The kinetics of M were measured by following the light-induced optical density (OD) change at 410 nm. Thus, the light-induced EPR changes could be correlated with specific intermediates during the second half of the photocycle. As expected, all the observed light-induced conformational changes were reversible. The comparisons between the observed changes and the photocycle kinetics are discussed below with respect to each spin-labeled mutant.

(A) S35R1 (A−B Interhelical Loop). The EPR spectral change for this mutant reaches its maximum amplitude shortly after the start of M decay, which is indicated by a decrease in the absorbance value at 410 nm (Figure 5a). The EPR signal subsequently decays with a slightly slower rate than that of M. Consequently, the structural change detected by the spin-label at this position appears to originate in M, but is associated with the M to N transition. However, as mentioned above, the EPR spectral change is very small and cannot reflect a major conformational change.

(B) D96A/V101R1 and A103R1 (C−D Interhelical Loop). As shown in Figure 5b, the light-induced EPR spectral change for D96A/V101R1 rises after the 410 nm absorbance (M formation) has reached its maximum value. This is in accordance with our previous analysis for V101R1 (*26*). However, the presence of a prolonged M allows us to observe that the EPR signal reaches its maximum amplitude well before the initiation of M decay (Figure 5b). These results

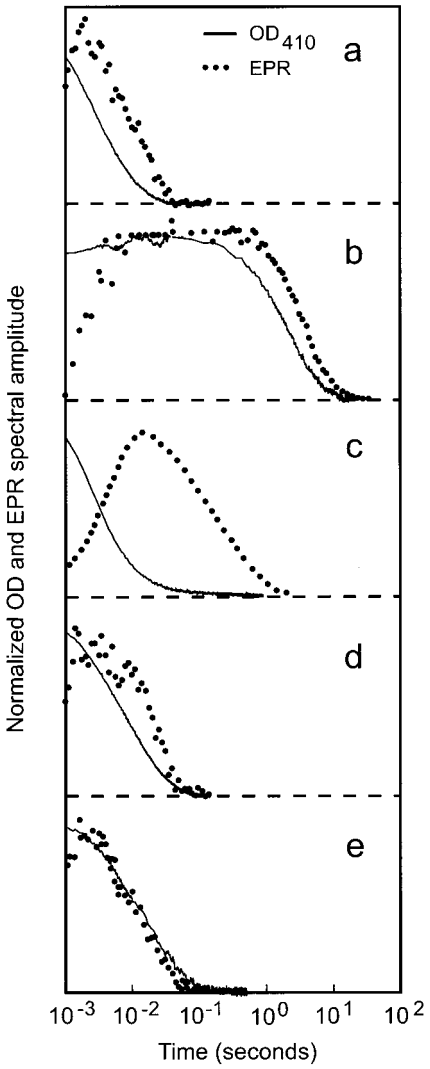

FIGURE 5: Normalized light-induced EPR spectral amplitudes (filled circles) and optical densities (OD) at 410 nm (solid lines) as a function of time for S35R1 (a), D96A/V101R1 (b), A103R1(c), V130R1 (d), and A160R1 (e). Changes in OD_{410nm} monitor M kinetics.

clearly demonstrate the existence of at least two protein conformations within the M intermediate, and show that a transition between these two M conformations involves movement at or near the C−D loop. The rate of decay of this conformational change is slower than the fast component of M decay but matches its slow component (Figure 5b).

Figure 5c shows the kinetics of the light-dependent EPR signal detected for A103R1. These kinetics are very similar to those observed for V101R1 (*26*). In addition, as discussed above, the EPR difference spectrum for A103R1 (Figure 4h) closely resembles that of V101R1 (dashed line in Figure 4g). These similarities suggest that the spin-label probe at site 103 is detecting the same conformational change as the probe attached to site 101 within the C−D interhelical loop. However, we cannot exclude the possibility that A103R1 is detecting either a completely different change or some additional changes that indeed occur during the M→N transition. This latter possibility is consistent with the reported occurrence of large amide bond changes during this step in the photocycle.

(C) V130R1 (D−E Interhelical Loop). It is difficult to obtain a precise correlation between the kinetics of the light-induced change at V130R1 and the kinetics of M because of the noise in the EPR signal. Nevertheless, it does appear that the EPR signal reaches its maximum value just as M decay has commenced and that, similar to S35R1, its own decay starts after the M decay is well under way (Figure 5d). Consequently, the detected movement appears to take place in M and be associated with transition to N. However, as pointed out above, the observed light-dependent change is small, and probably corresponds to a minor conformational change either at or in the vicinity of site 130.

(D) A160R1 (E−F Interhelical Loop). The transient EPR signal observed at A160R1 corresponds to a light-induced change that appears to occur in M, with a very similar time course to that for S35R1 and V130R1 (Figure 5e). However, in contrast with the two other sites, the timing of the EPR signal decay and the timing of M decay closely parallel one another. As with S35R1 and V130R1, the light-induced signal for A160R1 is weak, and probably corresponds to a small conformational change at or near the spin-label.

DISCUSSION

In the present work, we studied the R1 nitroxide side chain at sites within the A−B (35R1), C−D (101R1, 103R1), and E−F (160R1) interhelical loops at the cytoplasmic surface of BR. In addition, one site in the D−E interhelical loop (130R1) at the extracellular surface of the BR molecule was investigated (Figure 1).

The mobility of the R1 side chain in each of these mutants, as inferred from the spectral line shape, is strongly modulated by tertiary or quaternary contact interactions in which it is involved. For example, the R1 side chains at sites 35, 101, 103, 130, and 160 all show some evidence of contact interactions, because their spectra reflect immobilization relative to R1 on noninteracting helix surfaces or in loops (*49*). Because the BR used in these experiments is in the native two-dimensional lattice, either inter- or intramolecular contacts could be responsible for the immobilization.

In principle, these possibilities can be distinguished by comparing the EPR spectra for BR in the purple membrane and in the monomeric state. If the interactions are intramolecular, there should be no difference between the spectra for BR in the lattice and monomeric forms. For sites 101 and 103, the EPR spectra for the purple membrane forms (Figure 4) are similar to those reported previously for the monomeric species (*50*). This observation indicates that the interactions restricting the motion of the nitroxide side chains at these sites are intramolecular, and are not due to the interaction of the nitroxides with adjacent bR molecules in the lattice. For V130R1, the monomeric form (*44*) has a much higher R1 mobility compared to the lattice state, suggesting that the immobilization in the lattice is due to interactions between BR molecules within a trimer. For R1 at sites 35 and 160, the EPR spectrum of the monomeric form has not been recorded. However, Kimura et al. have obtained a structure for the E−F loop based on electron cryomicroscopy studies (*51*). In addition, Steinhoff and co-workers have provided a model for the E−F loop based on EPR studies of each residue in the unphotolyzed state of BR (*52*). The analysis of the latter work indicates that the interaction of the R1 side chain at site 160 is intramolecular.

In the set that we have examined, the photoinduced EPR transients reflecting a conformational change in BR are large

only for R1 at sites 101 and 103 in the C−D loop. Thorgeirsson et al. have also investigated the light-dependent changes for A103R1, but in contrast to our results found no light-induced EPR transients (*29*). This difference from our findings may be due to a lower sensitivity of their instrumental arrangement. The EPR transients for R1 at 35, 130, and 160 are much smaller than at 101 and 103. It is perhaps not surprising that only a small change is observed at position 130, because it is apparently on the outside surface of the protein, at a contact site between monomers in the lattice (Figure 1b). The small EPR transients at positions 35, 130, and 160 have a very similar time course corresponding to a light-induced change that appears in M (Figure 5). However, the timing relative to M differs. This may be because the M decay in A160R1 is slowed more than in V130R1, reflecting a greater shift in the M−N equilibrium toward the M state. Thus, the light-induced EPR transients for sites 35, 130, and 160 likely reflect the rise of the same conformational change during M and its subsequent decay during the recovery of the unphotolyzed state. However, the differences in M decay between the mutants may reflect differences in the M−N equilibrium and the amount of back-reaction from N to M. For all the examined sites, the exact nature of the observed movements remains to be determined.

A main purpose of the present study was to explore the correlation between the time course of the M intermediate and the light-dependent structural transition in BR detected by spin-labels in the C−D loop. In V101R1, similar to A103R1 (Figure 5c), the rise of the EPR transient coincides with M decay (*26*). Does this indicate a synergy between the observed protein motion and Schiff base reprotonation, or do the two events actually occur independently? To distinguish between these two possibilities, we examined the time course of the conformational change in a mutant with a greatly retarded M decay. In this mutant, D96A/V101R1, the EPR spectrum is virtually identical to V101R1 alone (Figure 4b), as is the spectral change under light excitation (Figure 4g). This convincingly shows that the D96A mutation does not affect the nature or magnitude of the conformational switch that occurs either at or near site 101. The data of Figure 5b for D96A/V101R1 demonstrate that the EPR spectral change rises after the complete formation of M and reaches maximum amplitude well before the start of M decay. Thus, the major conformational change detected by V101R1 occurs within the M intermediate, directly demonstrating the conformational heterogeneity of this state at neutral pH. These results also provide a precise time of occurrence for this conformational change which is clearly uncoupled from the Schiff base reprotonation even though these two events show an apparent coincidence in time when analyzed in the wild-type background.

Very recent time-resolved electron diffraction measurements for wild-type and mutant BR samples have revealed that the major light-induced conformational changes associated with transmembrane helices occur within approximately the first millisecond of the photocycle (*53*). We show in this report that our EPR data are consistent with this conclusion. The conformational change detected in D96A/V101R1 begins to accumulate 1 ms after the initiation of the photocycle (Figure 5b). Consequently, it could signify a response of the spin-label to the major light-induced changes seen by electron diffraction. It may also be the signature of a separate loop-specific motion that accompanies the observed diffraction changes in transmembrane regions (see below).

Sass et al. (*38*) and Subramaniam et al. (*53*) have interpreted their respective diffraction results as an indication that the major conformational transitions in BR occur in the proposed $M_1 \rightarrow M_2$ step (*32*). Both reports also conclude that the amide changes observed by FTIR do not correlate with tertiary structural changes that occur in M. Sass et al. (*38*) have made this determination based on FTIR and X-ray studies of the hydrated D96N mutant at high pH and of wild-type BR incubated with guanidine hydrochloride (*19*). They have therefore postulated that the additional amide change may signify a $M_2 \rightarrow M_N$ transition. To which of these proposed steps in M does the EPR change correspond? As discussed above, our EPR results are consistent with the diffraction data in terms of the timing of the detected conformational change. It is therefore reasonable to propose that the motion observed in D96A/V101R1 is correlated with the reported diffraction measurements. If indeed the observed diffraction changes occur in the $M_1 \rightarrow M_2$ step as proposed, then our EPR signal may correspond to this specific transition in M. However, further analysis is required to determine whether the observed EPR change corresponds to the $M_1 \rightarrow M_2$ or the $M_2 \rightarrow M_N$ transition, especially in light of the observation that at neutral pH M_N is present in the early M intermediate of the D96N mutant (*39*). If the detected EPR change turns out to be due to M_N formation, it would be the first direct evidence for the occurrence of M_N in wild-type BR as we have demonstrated that the same EPR change takes place in both V101R1 and D96A/V101R1 samples.

The structural origin of the light-induced EPR changes in 101R1 remains a matter for speculation. Based on modeling the spin-label position, we had previously suggested that it may originate from motion in the C−D and/or the E−F loop (*26*). The absence of a significant light-induced EPR transient for A160R1 during the photocycle argues against the E−F loop being the origin of such motion. It is possible that a particular orientation of the spin-label side chain at position 160 prevents it from detecting a significant conformational change. However, it should be noted that time-resolved EPR analysis of E161R1 also reveals only a small light-induced change (*28*). Although Thorgeirsson et al. (*29*) did not observe any change in A103R1, their instrument did detect a small light-induced change at position 163 (M163R1). However, we do not believe that this change originates in the E−F loop. The nitroxide at position 163 is oriented toward the inside of the protein between helices C and F whereas those at residues 160 and 161 point outward (*52*). Therefore, the observed change in M163R1 most likely reflects a significant movement in either helix C or helix F, or both. Such a large change would be easily detectable given the orientation of the spin-label at position 163. It may result in an increase in the interhelical distance between helices C and F, consistent with the observed increase in nitroxide mobility in M163R1 as a consequence of this movement. Preliminary X-ray analysis of D96A/V101C modified with a mercury atom suggests a movement of the C−D loop in the M state as indicated by a change in the position of the attached mercury.[2] If these results are verified, they would

[2] Ramin Mollaaghababa, Wolfgang Behrens, Ulrike Alexiev, H. Gobind Khorana, and Maarten Heyn, unpublished observation.

suggest that the light-induced EPR signal for site 101R1 is associated with a movement of the C−D interhelical loop. The observed movement may be part of a conformational change, which allows better access to the aqueous milieu either for efficient reprotonation of the Schiff base during the M to N transition or for efficient reprotonation of Asp 96 during N decay, or both. In this connection, it is noteworthy that a cavity seen under the C−D loop in electron diffraction analysis of BR can become accessible to solvent if the side chain of Asp 102 is rotated (*54*).

In summary, our results provide information regarding the lattice conformations of several BR loop regions both in the unphotolyzed and in the photolyzed states and thus extend the previous EPR studies (*26*, *28*, *29*). Most importantly, they provide time-resolved structural evidence that the occurrence of a major conformational change in M involves motion at or near the C−D loop. These findings reemphasize the versatility and utility of the EPR technique for time-resolved structural studies of membrane proteins such as bacteriorhodopsin.

REFERENCES

1. Oesterhelt, D., and Stoeckenius, W. (1971) *Nature 233*, 149−152.
2. Bayley, H., Huang, K.-S., Radhakrishnan, R., Ross, A. H., Takagaki, Y., and Khorana, H. G. (1981) *Proc. Natl. Acad. Sci. U.S.A. 78*, 2225−2229.
3. Stoeckenius, W., and Bogomolni, R. A. (1982) *Annu. Rev. Biochem. 51*, 587−616.
4. Khorana, H. G. (1988) *J. Biol. Chem. 263*, 7439−7442.
5. Lanyi, J. K. (1993) *Biochim. Biophys. Acta 1183*, 241−261.
6. Krebs, M. P., and Khorana, H. G. (1993) *J. Bacteriol. 175*, 1555−1560.
7. Oesterhelt, D. (1998) *Curr. Opin. Struct. Biol. 8*, 489−500.
8. Mogi, T., Stern, L. J., Marti, T., Chao, B. H., and Khorana, H. G. (1988) *Proc. Natl. Acad. Sci. U.S.A. 85*, 4148−4152.
9. Braiman, M. S., Mogi, T., Marti, T., Stern, L. J., Khorana, H. G., and Rothschild, K. J. (1988) *Biochemistry 27*, 8516−8520.
10. Subramaniam, S., Marti, T., and Khorana, H. G. (1990) *Proc. Natl. Acad. Sci. U.S.A. 87*, 1013−1017.
11. Otto, H., Marti, T., Holz, M., Mogi, T., Stern, L. J., Engel, F., Khorana, H. G., and Heyn, M. P. (1990) *Proc. Natl. Acad. Sci. U.S.A. 87*, 1018−1022.
12. Otto, H., Marti, T., Holz, M., Mogi, T., Lindau, M., Khorana, H. G., and Heyn, M. P. (1989) *Proc. Natl. Acad. Sci. U.S.A. 86*, 9228−9232.
13. Holz, M., Drachev, L. A., Mogi, T., Otto, H., Kaulen, A. D., Heyn, M. P., Skulachev, V. P., and Khorana, H. G. (1989) *Proc. Natl. Acad. Sci. U.S.A. 86*, 2167−2171.
14. Butt, H. J., Fendler, K., Bamberg, E., Tittor, J., and Oesterhelt, D. (1989) *EMBO J. 8*, 1657−1663.
15. Gerwert, K., Hess, B., Soppa, J., and Oesterhelt, D. (1989) *Proc. Natl. Acad. Sci. U.S.A. 86*, 4943−4947.
16. Rothschild, K. J. (1992) *J. Bioenerg. Biomembr. 24*, 147−167.
17. Koch, M. H. J., Dencher, N. A., Oesterhelt, D., Plohn, H.-J., Rapp, G., and Buldt, G. (1991) *EMBO J. 10*, 521−526.
18. Nakasako, M., Kataoka, M., Amemiya, Y., and Tokunaga, F. (1991) *FEBS Lett. 292*, 73−75.
19. Dencher, N. A., Heberle, J., Bark, C., Koch, M. H. J., Rapp, G., Oesterhelt, D., Bartels, K., and Buldt, G. (1991) *Photochem. Photobiol. 54*, 881−887.
20. Subramaniam, S., Gerstein, M., Oesterhelt, D., and Henderson, R. (1993) *EMBO J. 12*, 1−8.
21. Han, B.-G., Vonck, J., and Glaeser, R. M. (1994) *Biophys. J. 67*, 1179−1186.
22. Dencher, N. A., Dresselhaus, D., Zaccai, G., and Buldt, G. (1989) *Proc. Natl. Acad. Sci. U.S.A. 86*, 7876−7879.
23. Subramaniam, S., Faruqi, A. R., Oesterhelt, D., and Henderson, R. (1997) *Proc. Natl. Acad. Sci. U.S.A. 94*, 1767−1772.
24. Hubbell, W. L., and Altenbach, C. (1994) *Curr. Opin. Struct. Biol. 4*, 566−573.
25. Hubbell, W. L., Mchaourab, H. S., Altenbach, C., and Lietzow, M. A. (1996) *Structure 4*, 779−783.
26. Steinhoff, H.-J., Mollaaghababa, R., Altenbach, C., Hideg, K., Krebs, M. P., Khorana, H. G., and Hubbell, W. L. (1994) *Science 266*, 105−107.
27. Steinhoff, H.-J., Mollaaghababa, R., Altenbach, C., Khorana, H. G., and Hubbell, W. L. (1995) *Biophys. Chem. 56*, 89−94.
28. Rink, T., Riesle, J., Oesterhelt, D., Gerwert, K., and Steinhoff, H.-J. (1997) *Biophys. J. 73*, 983−993.
29. Thorgeirsson, T. E., Xiao, W., Brown, L. S., Needleman, R., Lanyi, J. K., and Shin, Y.-K. (1997) *J. Mol. Biol. 273*, 951−957.
30. Hess, B., and Kuschmitz, D. (1977) *FEBS Lett. 74*, 20−24.
31. Li, Q.-Q., Govindjee, R., and Ebrey, T. G. (1984) *Proc. Natl. Acad. Sci. U.S.A. 81*, 7079−7082.
32. Varo, G., and Lanyi, J. K. (1990) *Biochemistry 29*, 2241−2250.
33. Druckmann, S., Friedman, N., Lanyi, J. K., Needleman, R., Ottolenghi, M., and Sheves, M. (1992) *Photochem. Photobiol. 56*, 1041−1047.
34. Friedman, N., Gat, Y., Sheves, M., and Ottolenghi, M. (1994) *Biochemistry 33*, 14758−14767.
35. Sasaki, J., Shichida, Y., Lanyi, J. K., and Maeda, A. (1992) *J. Biol. Chem. 267*, 20782−20786.
36. Vonck, J., Han, B.-G., Burkard, F., Perkins, G. A., and Glaeser, R. M. (1994) *Biophys. J. 67*, 1173−1178.
37. Weik, M., Zaccai, G., Dencher, N. A., Oesterhelt, D., and Hauss, T. (1998) *J. Mol. Biol. 275*, 625−634.
38. Sass, H. J., Schachowa, I. W., Rapp, G., Koch, M. H. J., Oesterhelt, D., Dencher, N. A., and Buldt, G. (1997) *EMBO J. 16*, 1484−1491.
39. Rodig, C., and Siebert, F. (1999) *FEBS Lett. 445*, 14−18.
40. Kita, T., Brown, M. S., and Goldstein, J. L. (1980) *J. Clin. Invest. 66*, 1094−1100.
41. Krebs, M. P., Mollaaghababa, R., and Khorana, H. G. (1993) *Proc. Natl. Acad. Sci. U.S.A. 90*, 1987−1991.
42. Krebs, M. P., Hauss, T., Heyn, M. P., RajBhandary, U. L., and Khorana, H. G. (1991) *Proc. Natl. Acad. Sci. U.S.A. 88*, 859−863.
43. Scherrer, P., Alexiev, U., Otto, H., Heyn, M. P., Marti, T., and Khorana, H. G. (1994) *Biochemistry 33*, 13684−13692.
44. Altenbach, C., Marti, T., Khorana, H. G., and Hubbell, W. L. (1990) *Science 248*, 1088−1092.
45. Laemmli, U. K. (1970) *Nature 227*, 680−685.
46. Rehorek, M., and Heyn, M. P. (1979) *Biochemistry 18*, 4977−4983.
47. Mollaaghababa, R. (1995) Ph.D. Thesis, Massachusetts Institute of Technology.
48. Alexiev, U., Mollaaghababa, R., Scherrer, P., Khorana, H. G., and Heyn, M. P. (1995) *Proc. Natl. Acad. Sci. U.S.A. 92*, 372−376.
49. Mchaourab, H. S., Lietzow, M. A., Hideg, K., and Hubbell, W. L. (1996) *Biochemistry 35*, 7692−7704.
50. Greenhalgh, D. A., Altenbach, C., Hubbell, W. L., and Khorana, H. G. (1991) *Proc. Natl. Acad. Sci. U.S.A. 88*, 8626−8630.
51. Kimura, Y., Vassylyev, D. G., Miyazawa, A., Kidera, A., Matsushima, M., Mitsuoka, K., Murata, K., Hirai, T., and Fujiyoshi, Y. (1997) *Nature 389*, 206−211.
52. Pfeiffer, M., Rink, T., Gerwert, K., Oesterhelt, D., and Steinhoff, H.-J. (1999) *J. Mol. Biol. 287*, 163−171.
53. Subramaniam, S., Lindahl, M., Bullough, P., Faruqi, A. R., Tittor, J., Oesterhelt, D., Brown, L., Lanyi, J., and Henderson, R. (1999) *J. Mol. Biol. 287*, 145−161.
54. Grigorieff, N., Ceska, T. A., Downing, K. H., Baldwin, J. M., and Henderson, R. (1996) *J. Mol. Biol. 259*, 393−421.
55. Essen, L. O., Siegert, R., Lehmann, W. D., and Osterhelt, D. (1998) *Proc. Natl. Acad. Sci. U.S.A. 95*, 11673−11678.

BI991963H